International Journal of Neuroscience, 119:639–663, 2009

ISSN: 0020-7454 / 1543-5245 online
DOI: 10.1080/00207450802325561

informa
healthcare

MOVEMENT-RELATED CORTICAL EVOKED POTENTIALS USING FOUR-LIMB IMAGERY

A. SANO

School of Fundamental Science and Technology
Graduate School of Science and Technology
Keio University
Yokohama, Kanagawa, Japan

H. BAKARDJIAN

Laboratory for Advanced Brain Signal Processing
Brain Science Institute
RIKEN
Wako-shi, Saitama, Japan

We compared the electroencephalographic changes during actual and imaginary movements with four limbs and classified optimally the responses during four-limb imagery. Evoked potentials in imagery exhibited lower and delayed peaks compared to actual-movement responses, but activations in the primary and the supplementary motor area were similar. Source-modeling analysis revealed that the motor and the parietal cortex were activated similarly, but several dipole sources were active in the frontal cortex for imagery. We compared thirteen classification methods and a combination of template matching and time-frequency methods showed the highest average of 70% classification rate for all limbs.

Keywords brain computer interface (BCI), electroencephalogram (EEG), hand, foot, imaginary movement, motor imagery

INTRODUCTION

Body movement is one of the most basic activities in our daily lives. Humans are able to perform the most suitable movement trajectories with

Received 6 March 2008.

Address correspondence to Akane Sano, 3-14-1 Hiyoshi, Kohoku-Ku, Yokohama, Kanagawa, Japan 223-8522. E-mail: akane_bme@hotmail.com

astonishing precision, for example when reaching for moving objects, to walk, to change their posture and to write. These activities are made possible by their highly adaptive motor system, which is finely controlled by the central and peripheral nervous systems, with very little need for conscious efforts and prior calculations.

In addition to various aspects of the brain activities during actual movements, those during imaginary movements have been also studied in detail in the past (Fadiga, et al., 1999). One of the main reasons for the interest in brain activity comparisons between execution and imagination of movements is that it is still controversial to what extent the supplementary motor cortex (SMA) and the primary motor cortex (MI) are activated in these two movement conditions. Apart from the classical concept that the SMA regulates the preparation of movements and MI controls their actual execution (Brunner, Scherer, Graimann, Supp, & Pfurtscheller, 2006; Clark, Tremblay, & Ste-Marie, 2004), recent evidence shows that the roles of these cortical areas especially during motor imagery may be more complex. Rodríguez, Muñiz, González, and Sabaté (2004) demonstrated broader and more intense cortical response modifications in MI during motor tasks not accompanied by movements than during the execution of simple motor acts.

Another important reason for the interest in imaginary movements is their application to brain computer interfaces. A brain computer interface (BCI), most often implemented by using noninvasive electroencephalographic (EEG) signal acquisition, is a connection between a human and a computer for the purpose of relaying commands to the computer without the activation of any body muscles. More formally, BCI is defined as "a communication system that does not depend on the brain's normal output pathways of peripheral nerves and muscles" (Wolpaw, Birbaumer, Heetderks, McFarland, & Peckham, 2000). At the present level of technology in developed countries, healthy humans often manipulate devices in their daily lives by pressing buttons. However, for individuals who cannot control any or some of their muscles due to amyotrophic lateral sclerosis (ALS), spinal cord injury or severe stroke, this is difficult to do. There is an urgent need to establish another way for device control and human communications for such disabled individuals, and BCI is the most promising alternative to reach that goal. Control of remote devices by imagination can be achieved either by surgically implanting electrodes on the surface or inside the brain, or by noninvasive cortical signal measurements, such as the classification system developed by Pfurtscheller and Lopes da Silva (1999), which is able to work in real time by utilizing event-related (de-)synchronization changes during imaginary movements. Noninvasive BCI studies usually attempt to

use various EEG features as input triggers for control—frequency-domain subbands (mu-rhythm, beta-rhythm, etc.) and time-domain signal parameters (slow cortical potentials or P300 potentials) (Anderson, Stolz, & Shamsunder, 1998; Leuthardt, Schalk, Wolpaw, Ojemann, & Moran, 2004; Neumann, Kaiser, Kotchoubey, Hinterberger, & Birbaumer, 2001; Obermaier, Neuper, Guger, & Pfurtscheller, 2001; Pham et al., 2005; Sellers & Donchin, 2006; Wolpaw & McFarland, 2004). The latest study with the highest classification rate is between 60% and 66.7% for three mental states (motor imagery of left hand, right hand, and foot with single-trial accuracies) (Brunner et al., 2006).

Robust EEG responses from the motor cortex can be used in a number of applications. In patients with motor disorders such as Parkinson's disease and hemiplegia, improved diagnosis could be achieved through evaluation of various parameters of motor activity (Filipovic et al., 2001; Platz et al., 2000).

In both healthy individuals and patients, processed cortical signals related to imaginary body-part movements could serve as interfaces for manipulation of cursor movements, for typing text, or for icon selection on a computer as well as for device control, robotic limbs, functional electric stimulation devices, and entertainment systems (Wolpaw, Birbaumer, McFarland, Pfurtscheller, & Vaughan, 2002).

Although numerous BCI studies have been conducted in recent years, there are only a few publications attempting a classification using more than two limbs (Brunner et al., 2006; Pfurtscheller, Brunner, Schlogl, & Lopes da Silva, 2006). In addition, most of the BCI classification methods in the scientific literature use learning systems such as neural networks, in which the researcher has little control or understanding over the classifier's "black box" output.

In this study, we investigated EEG responses acquired during actual and imaginary four-limb movements in healthy humans. Our objectives were (1) to compare the EEG responses before, during, and after actual and imaginary movements to clarify the cortical activation differences in the actual and imaginary limb movements, and (2) to classify the EEG responses in all four experimental conditions—imaginary movements with right hand, left hand, right leg, and left leg. Our classification approach is the result of a specific need for a fast and fully transparent BCI algorithm for unsupervised usage in practical applications in which the limb-recognition winner was selected from thirteen competing methods.

EXPERIMENTAL PROCEDURES

The experiments were performed with three right-handed subjects without a history of neuromuscular and neurological disorders. A whole-head 64-channel EEG System (NeuroScan SynAmps, Compumedics, Abbotsford, Australia) was applied for measuring 56-channel EEG signals based on the extended 10/20 International System. Eight additional channels were used to acquire surface-EMG signals (extensor carpi radialis longus muscles and tibialis anterior muscles) from the four limbs. The EEG sampling frequency was 1 kHz and the data was recorded in the 0.05–200 Hz frequency range. The subjects were seated on a comfortable chair in an electrically, acoustically, and visually shielded room while performing the experiments. They were shown small white circles on a black background displayed for 0.05 s at random intervals between 5 and 8 s as visual cues to execute alternatively actual and imaginary movements of wrist extension and ankle dorsiflexion by bending the relevant limb joints (articulatio radiocarpalis, and articulatio talocruralis). Breaks were introduced for relaxation. The duration of each session was about 10 minutes for 120 trials and, in total, 10 sessions per subject were conducted.

ANALYSIS

EEG Responses

In general, EEG responses can be classified into two types according to the way they respond to sensory stimulation. One type represents time-locked and phase-locked responses, also known as event-related potentials (ERP). These are the responses of stationary or quasi-stationary cortical subsystems to the external stimuli, as a result of the existing neuronal networks in the cortex. The other type is time-locked but not phase-locked (induced) modulation, called event-related (de-)synchronization (ERD(S)). It can be measured due to alterations in the functional connectivity within the cortex. Different analytical methods should be used for these two types of EEG changes. Evoked activities can be enhanced and extracted using simple linear methods, for example, based on synchronous averaging, while induced activities should be analyzed using nonlinear methods such as those based on power spectral analysis and rectified averaging.

During the signal preprocessing step, we applied a 0.5–40 Hz band-pass filter to the recorded EEG signals and generated single trials each starting 2.5 s before the cue and ending 2.5 s after the cue. After eliminating all trials with strong noise, we aligned the onsets of the visual stimuli and calculated the

50-trial averaged EEG responses to determine the standard ERP waveforms for phase-locked responses. In addition, we estimated the ERD(S) by calculating all single-trial time-frequency arrays and averaging for each condition. Finally, we modeled and extracted the location of the activated cortical sources on the basis of the surface EEG from 96 ms to 505 ms using discrete equivalent dipole analysis (BESA, MEGIS Software, Gräfelfing, Germany) in which a genetic fit search algorithm minimized the error between the measured and modeled EEG data. We applied a four-shell ellipsoidal volume conductor model of the head, and the percentage of the data, which could not be described when the model was evaluated by a residual variance measure (<5%). Each source dipole estimated the electrical activity in a patch of cortex, and was described by seven parameters—the x, y, z location, the x, y, z orientation, and the dipole moment.

EEG Classification

Classification Methods

For classification purposes, a single 50-trial average (template signal) and five 10-trial consecutive average (test signals) were randomly composed for each of the eight conditions. We applied and compared thirteen different methods for classification (shown later) that focuses ERP and ERD(S), as well as four variants. The largest or the smallest evaluation function comparing the EEG templates and their corresponding test signals were computed for each classification method (Yom-Tov & Inbar, 2003).

x_i^j: test signal (10-trial average, band-pass filtered signal).
y_i^j: template signal (50-trial average, band-pass filtered signal).
$i = 1, \ldots, n$: number of data samples.
$j = 1, \ldots, 5$: number of electrodes (F3, F4, C3, Cz, C4).

Method (1): *Signal Amplitude Root Mean Square (RMS) Error*

This method uses the RMS measure calculated using the test signal (10-trial block) and the template (50-trial block), averaged across five scalp locations.

$$J^j = \sum_{i=1}^{n} \left(y_i^j - x_i^j\right)^2. \tag{1}$$

$$J = \sum_{j=1}^{5} (J^j). \tag{2}$$

$$\text{Winner: } \min(J). \tag{3}$$

Method (2): *Five-Dimensional RMS Vector Angle*

This method applies the degree between RMS vectors of the test signal and the template averaged across five scalp locations.

$$\mathrm{RMS}^j = \sqrt{\frac{1}{n}\sum_{i=1}^{n}\left(x_i^j - \overline{x^j}\right)^2}. \tag{4}$$

$$a = \mathrm{RMS}_{\mathrm{temp}} = \left[\mathrm{RMS}^1_{\mathrm{temp}}, \mathrm{RMS}^2_{\mathrm{temp}}, \ldots, \mathrm{RMS}^5_{\mathrm{temp}}\right]. \tag{5}$$

$$b = \mathrm{RMS}_{\mathrm{unknown}} = \left[\mathrm{RMS}^1_{\mathrm{unknown}}, \mathrm{RMS}^2_{\mathrm{unknown}}, \ldots, \mathrm{RMS}^5_{\mathrm{unknown}}\right]. \tag{6}$$

$$\theta = \cos^{-1}\left(\frac{a \cdot b}{|a||b|}\right). \tag{7}$$

$$\text{Winner: } \min(\theta). \tag{8}$$

Method (3): *Pearson Correlation between a Template and a Test Trial*

This method uses the correlation between the test signal and the template averaged across five scalp locations.

$$C^j = \frac{\text{Covariance between unknown signal and template}}{\text{Standard deviation of unknown signal} \times \text{Standard deviation of template}}$$

$$= \frac{\frac{1}{n}\sum_{i=1}^{n}\left(x_i^j - \overline{x^j}\right)\left(y_i^j - \overline{y^j}\right)}{\sqrt{\frac{1}{n}\sum_{i=1}^{n}\left(x_i^j - \overline{x^j}\right)^2}\sqrt{\frac{1}{n}\sum_{i=1}^{n}\left(y_i^j - \overline{y^j}\right)^2}}, \tag{9}$$

where $\overline{y}^j = \dfrac{1}{n}\sum_{i=1}^{n} y_i^j$ stands for the mean value of y_i^j $(j = 1, \ldots, n)$.

$$C = \sum_{j=1}^{5}(C^j)^2. \tag{10}$$

$$\text{Winner: } \max(C) \tag{11}$$

Method (4): *Pearson Correlation between Sensors*

This method employs the RMS difference of the correlations between scalp locations comparing the test signal and the template.

$$C_{\text{int}}^{jh} = \frac{\text{Covariance between Electrode (j) and Electrode (h)}}{\text{Standard Deviation of Electrode (j)} \times \text{Standard Deviation of Electrode (h)}}$$

$$= \frac{\frac{1}{n}\sum_{i=1}^{n}\left(x_i^j - \overline{x^j}\right)\left(x_i^h - \overline{x^h}\right)}{\sqrt{\frac{1}{n}\sum_{i=1}^{n}\left(x_i^j - \overline{x^j}\right)^2}\sqrt{\frac{1}{n}\sum_{i=1}^{n}\left(x_i^h - \overline{x^h}\right)^2}}. \tag{12}$$

$$C_{\text{int}} = \sum_{j=1}^{5}\sum_{h=1}^{5}\left(C_{\text{int\_temp}}^{jh} - C_{\text{int\_unknown}}^{jh}\right)^2. \tag{13}$$

$$\text{Winner: } \min(C_{\text{int}}) \tag{14}$$

Method (5): *Time-Frequency RMS Error*

This method uses the RMS difference in the time-frequency power spectrum (0.5 Hz–40 Hz) between the test signal and the template averaged across five scalp locations.

$$p_{\text{temp}_{if}^j} = \sum_{j=1}^{5}\sum_{f=0.5}^{40}\sum_{i=1}^{n} x_i^j e^{-\text{j}2\pi f}. \tag{15}$$

$$L = \sum_{j=1}^{5}\sum_{i=1}^{n}\sum_{f=0.5}^{40}\left(p_{\text{temp}_{if}^j} - p_{\text{unknown}_{if}^j}\right)^2. \tag{16}$$

$$\text{Winner: } \min(L) \tag{17}$$

Method (6): *Frequency-Band Time-Frequency RMS Error*

This method employs the RMS difference in the time-frequency power spectrum for theta, alpha, beta, and gamma bands between the test signal and the template averaged across five scalp locations.

$$p_{\text{temp}_{\text{iband}}^j} = \sum_{f=a}^{b} p_{\text{temp}_{if}^j}. \tag{18}$$

$$\begin{aligned} &p_{\text{temp}_{\text{iband}}^j} \\ &= \left[p_{\text{temp}_{if|_4^8}^j}, p_{\text{temp}_{if|_8^{12}}^j}, p_{\text{temp}_{if|_{12}^{30}}^j}, p_{\text{temp}_{if|_{30}^{40}}^j}\right] \\ &= \left[p_{\text{temp}_{i\text{theta}}^j}, p_{\text{temp}_{i\text{alpha}}^j}, p_{\text{temp}_{i\text{beta}}^j}, p_{\text{temp}_{i\text{gamma}}^j}\right]. \end{aligned} \tag{19}$$

The same calculation is conducted for test signals to obtain $p_{\text{unknown}^j_{i\text{band}}}$.

$$L_{\text{band}} = \sum_{j=1}^{5}\sum_{i=1}^{n}\left(p_{\text{temp}^j_{i\text{band}}} - p_{\text{unknown}^j_{i\text{band}}}\right)^2. \tag{20}$$

$$\text{Winner: } \min(L_{\text{band}})$$

Method (7): *Alpha-Band (8–12 Hz) Time-Frequency RMS Error*

This method applies the RMS difference in the time-frequency power spectrum for alpha band between the test signal and the template averaged across five scalp locations.

$$\begin{aligned} &p_{\text{temp}^j_{i\text{alphaband}}} \\ &= p_{\text{temp}^j_{if|_8^{12}}}. \end{aligned} \tag{21}$$

The same calculation is conducted for test signals to obtain $p_{\text{unknown}^j_{i\text{alphaband}}}$.

$$L_{\text{alphaband}} = \sum_{j=1}^{5}\sum_{i=1}^{n}\left(p_{\text{temp}^j_{i\text{alphaband}}} - p_{\text{unknown}^j_{i\text{alphaband}}}\right)^2. \tag{22}$$

$$\text{Winner: } \min(L_{\text{alphaband}}) \tag{23}$$

Method (8): *Alpha–Beta Band (8–30 Hz) Time-Frequency RMS Error*

This method employs the RMS difference in the time-frequency power spectrum for alpha and beta bands between the test signal and the template averaged across five scalp locations.

$$\begin{aligned} &p_{\text{temp}^j_{i\text{band}}} \\ &= \left[p_{\text{temp}^j_{if|_8^{12}}}, p_{\text{temp}^j_{if|_{12}^{30}}}\right] \\ &= \left[p_{\text{temp}^j_{i\text{alpha}}}, p_{\text{temp}^j_{i\text{beta}}}\right]. \end{aligned} \tag{24}$$

The same calculation is conducted for test signals to obtain $p^j_{\text{unknown}} i_{\text{band}}$.

$$L_{\text{band}} = \sum_{j=1}^{5}\sum_{i=1}^{n}\left(p_{\text{temp}^j_{i\text{band}}} - p_{\text{unknown}^j_{i\text{band}}}\right)^2. \tag{25}$$

$$\text{Winner: } \min(L_{\text{band}}) \tag{26}$$

Method (9): *Frequency-Band Pearson Correlation between a Template and a Test Trial*

This method uses the correlation of the time-frequency power spectra for theta, alpha, beta, and gamma bands between the test signal and the template averaged across five scalp locations.

$$K^j = \frac{\text{Covariance between power of template and that of unknown signal}}{\text{Standard Deviation of power of template} \times \text{Standard Deviation of power of unknown signal}}$$

$$= \sum_{m=1}^{4} \left(\frac{\frac{1}{n}\sum_{i=1}^{n} \left(p_{\text{temp}^j_{\text{iband(m)}}} - \overline{p_{\text{temp}^j_{\text{iband(m)}}}}\right)\left(p_{\text{unknown}^j_{\text{iband(m)}}} - \overline{p_{\text{unknown}^j_{\text{iband(m)}}}}\right)}{\sqrt{\frac{1}{n}\sum_{i=1}^{n} \left(p_{\text{temp}^j_{\text{iband(m)}}} - \overline{p_{\text{temp}^j_{\text{iband(m)}}}}\right)^2}\sqrt{\frac{1}{n}\sum_{i=1}^{n} \left(p_{\text{unknown}^j_{\text{iband(m)}}} - \overline{p_{\text{unknown}^j_{\text{iband(m)}}}}\right)^2}} \right)^2 \tag{27}$$

$$\text{band} = [\text{theta},\ \text{alpha},\ \text{beta},\ \text{gamma}]. \tag{28}$$

$$K = \sum_{j}^{5} K^j. \tag{29}$$

$$\text{Winner: } \max(K). \tag{30}$$

During the calculation of the frequency bands for the time-frequency analysis, all 15 combinations were calculated using the following four bands—theta, alpha, beta, and gamma.

Method (10): *Pearson Correlation and Signal Amplitude RMS Error*

Combination of Method 1 and Method 3.

$$\text{Winner: } \max\left(C + \frac{1}{J}\right). \tag{31}$$

Method (11): *Signal Amplitude RMS Error and Time-Frequency RMS Error*

Combination of Method 1 and Method 5.

$$\text{Winner: } \min(L + J) \tag{32}$$

Method (12): *Time-Frequency RMS Error and Alpha–Beta band (8–20 Hz) Time-Frequency RMS Error*

Combination of Method 5 and Method 8.

$$\text{Winner: } \min(L + L_{\text{band}}) \tag{33}$$

Method (13): *Time-Frequency RMS Error and Frequency-Band Pearson Correlation between a Template and a Test Trial*

Combination of Method 10 and 11.

$$\text{Winner: } \max\left(K + \frac{1}{L_{\text{band}}}\right) \tag{34}$$

Matching Analysis. In order to identify the degree of matching between templates and test trials, we evaluated dynamically the transient similarity (a) between each actual-movement template and its corresponding five 10-trial actual-movement blocks, (b) between each imaginary-movement template and its corresponding five 10-trial imaginary-movement blocks, and (c) between each actual-movement template and its corresponding ten 10-trial imaginary-movement blocks. We calculated the RMS error in the time-frequency power spectrum between the template and test blocks across five scalp locations as given below.

$$p_{\text{temp}_{if}^{j}} = \sum_{j=1}^{5} \sum_{f=0.5}^{40} \sum_{i=1}^{n} x_i^j e^{-\text{j}2\pi f}, \tag{35}$$

$$\text{mismatch} = \sum_{j=1}^{5} \sum_{i=1}^{n} \sum_{f=0.5}^{40} \left(p_{\text{temp}_{if}^{j}} - p_{\text{test}_{if}^{j}}\right)^2. \tag{36}$$

The purpose of this type of analysis was not only to study neurophysiological associations in the actual- and imaginary-movement conditions, but also to gain additional knowledge about the efficiency of EEG-based motor BCI classification.

RESULTS

EEG Responses

Electrophysiological differences between actual- and imaginary-movement responses for electrode F3, Fz, F4, C3, Cz, and C4 are shown in Figure 1. Actual-movement post-cue responses exhibited slightly larger negative peak amplitude than imaginary-movement responses. Peak amplitudes were larger in left and central hemisphere electrodes in imaginary movements. EEG responses for imaginary movements seemed to be delayed compared to those for actual movement. Potentials from the frontal and central cortex were similar both in actual and imaginary movements.

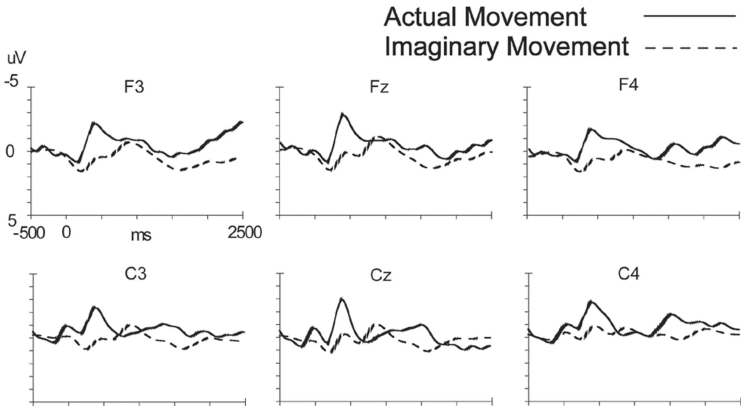

Figure 1. Comparison of EEG responses for right-hand actual movement (dashed line) and imaginary movement (solid line) at electrode F3, Fz, F4, C3, Cz, C4.

The outcome of the time-frequency plots of the 50-trial EEG averages from electrodes Fp1, Fp2, F3, Fz, F4, C3, Cz, C4, P3, P4, O1, and O2 is illustrated in Figure 2. Time-frequency analysis showed that actual movements exhibited theta activity in the frontal cortex as well as alpha, beta, and gamma post-cue activity in the motor and the posterior cortices. For imaginary movements, time-frequency decomposition revealed enhanced theta frequency-band activity immediately after the cue, accompanied by augmented beta- and gamma-band responses. Time-frequency results showed that the frontal and central cortex were both activated, but unlike in evoked potentials, ERD(S) analysis demonstrated more diverse activation patterns.

Figure 3 illustrates the averaged EEG responses (50 repetitions) for all four imaginary limb movements at electrode positions C3 and F4. Even for imaginary movements, the amplitudes of left-hand potentials were largest in the right hemisphere. We observed the left hand and foot movements showed large potential area between 0 and 2500 ms in F4.

Classification Results

Table 1 showed the classification rates for ten 10-trial test signals of imaginary movements for all four limbs using various data algorithms that rely on the 50-trial template of actual movements. The method evaluating the root-mean square (RMS) errors in the time-frequency plane showed the best mean

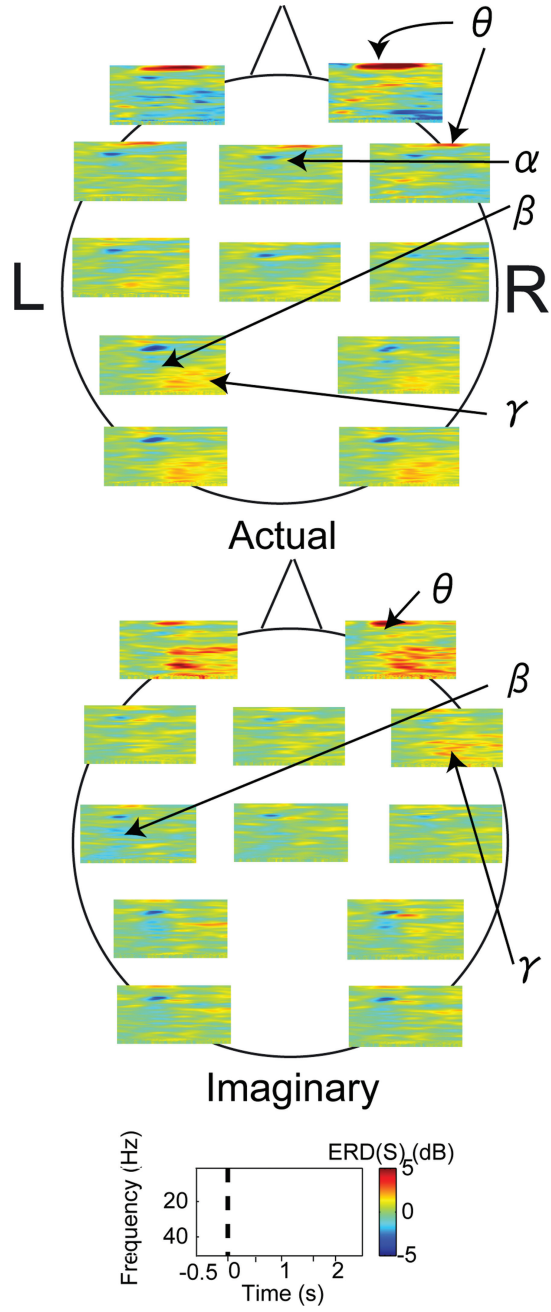

Figure 2. Results of the time-frequency analysis for actual and imaginary movements.

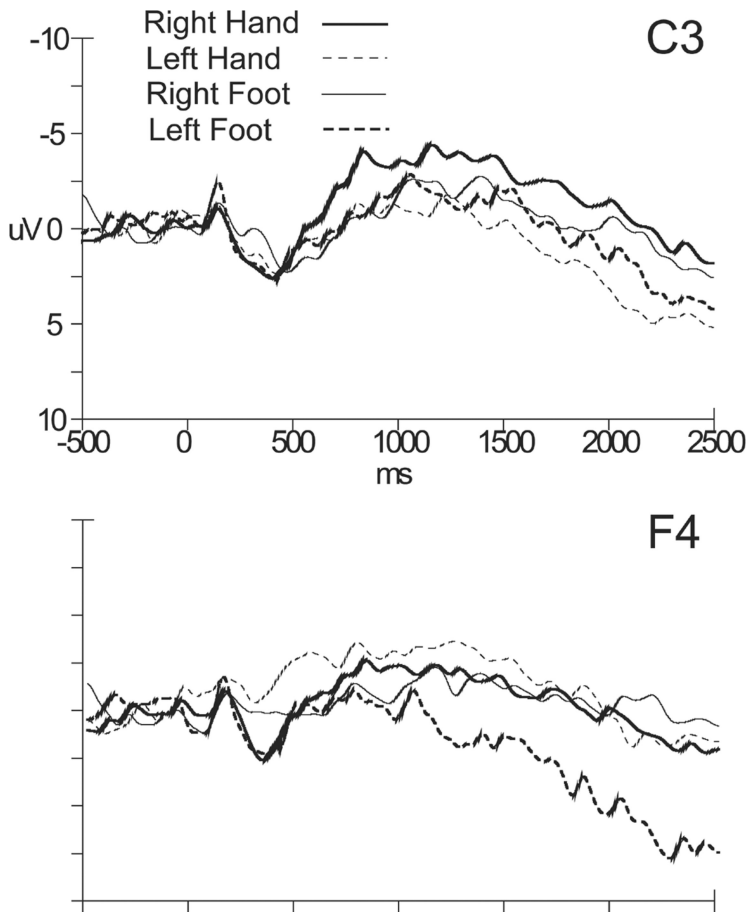

Figure 3. Comparison of EEG responses for all four conditions of imaginary limb movement at electrodes F4 and C3.

performance (70%), while the five-dimensional RMS Vector Angle method showed the worst mean performance (27.5%).

Matching Analysis

We investigated also the transient matching changes between the actual-movement template and, sequentially, all 10-trial test blocks of actual movement (A–A matching) (Figure 4), between the imaginary-movement template and all 10-trial test blocks of imaginary movement (I–I matching) (Figure 5), as well as between the actual-movement template and all

Table 1. Classification rates (in percent) for thirteen BCI data-evaluation methods, ordered for efficiency

Imaginary-movement condition method	Right hand	Left hand	Right leg	Left leg	Mean rate
12) Time-Frequency RMS Error and Alpha–Beta-band (8–30 Hz) Time-Frequency RMS Error	80	60	60	70	70
5) Time-Frequency RMS Error	60	60	70	80	67.5
8) Alpha-Beta band (8–20 Hz) Time-Frequency RMS Error	70	70	50	50	60
11) Signal Amplitude RMS Error and Time-Frequency RMS Error	60	50	60	40	52.5
13) Time-Frequency RMS Error and Frequency-Band Pearson Correlation between a Template and a Test Trial	60	50	60	40	52.5
3) Pearson Correlation Between a Template and a Test Trial	60	50	40	40	47.5
10) Pearson Correlation and Signal Amplitude RMS Error	60	50	20	40	42.5
7) Alpha-band (8–12 Hz) Time-Frequency RMS Error	50	40	50	30	42.5
1) Signal-Amplitude RMS Error	60	40	40	20	40
4) Pearson Correlation Between Sensors	50	10	50	40	37.5
9) Frequency-Band Pearson Correlation between a Template and a Test Trial	40	20	20	50	32.5
6) Frequency-band Time-Frequency RMS Error	30	10	50	30	30
2) Five-Dimensional RMS Vector Angle	20	30	30	30	27.5

10-trial test blocks of imaginary movement (A–I matching) (Figure 6). Figure 7 shows the summary of the mean and standard deviation mismatch values for all three utilized matching analyses in the time-frequency plane (A–A, I–I and A–I).

When comparing imaginary-movement templates with their corresponding 10-trial test blocks of imaginary movement (I–I matching), the right hand and the right leg exhibited a better mean match than the left hand and the left

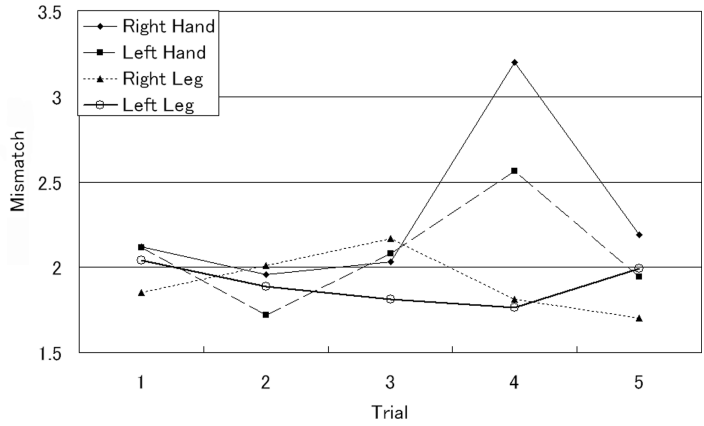

Figure 4. Actual–Actual transient matching consistency for all four limb-movement conditions. Here the actual-movement EEG data template is matched to the actual-movement 10-trial test blocks (A–A matching).

leg. For actual movements (A–A matching), leg responses showed greater consistency between their templates and the test-trial blocks than the hand responses. However, when comparing actual-movement templates to test blocks of imaginary limb movements (A–I matching), hands exhibited better mean matching than legs. Comparison of the trial-block variability for these three

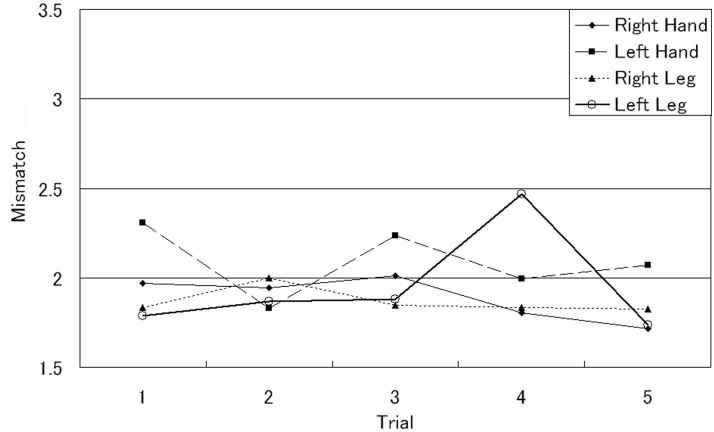

Figure 5. Imaginary–Imaginary transient matching consistency for all four limb-movement conditions. Here the imaginary-movement EEG data template is matched to the imaginary-movement 10-trial test blocks (I–I matching).

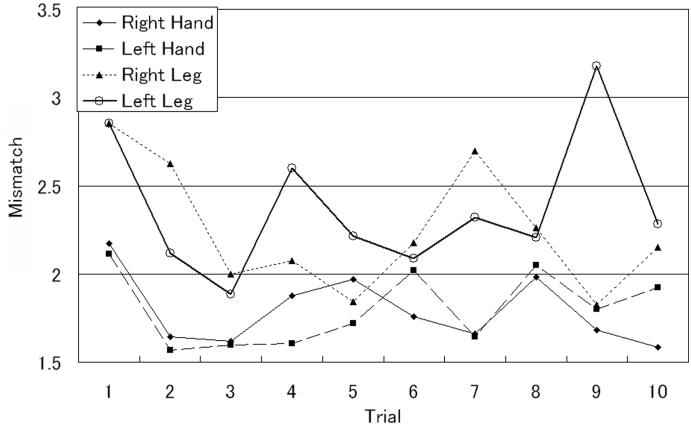

Figure 6. Actual–Imaginary transient matching consistency for all four limb-movement conditions. Here the actual-movement EEG data template is matched to the imaginary-movement 10-trial test blocks (A–I matching).

matching types showed that A–A matching was highly variable in the right hand and A–I matching was the most variable in the right leg (F-statistics, $p < 0.05$). In A–I matching, the template-test similarities reached a maximum after 20–30 repetitions, after which the response variability increased.

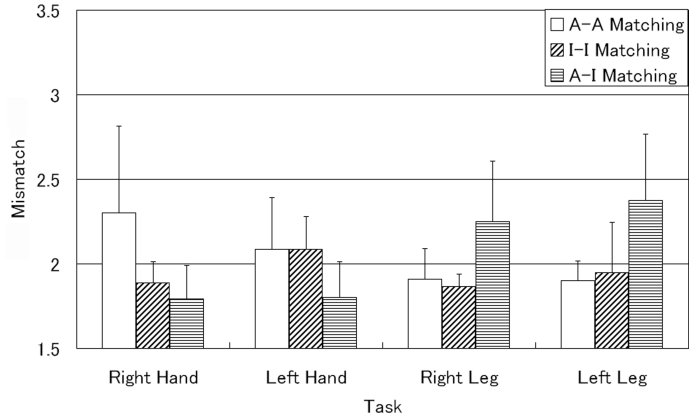

Figure 7. Comparison of the mean and standard deviation matching values between imaginary-movement templates and imaginary-test trials (I–I matching), between actual-movement templates and actual-test trials (A–A matching), and between actual-movement templates and imaginary-test trials (A–I matching).

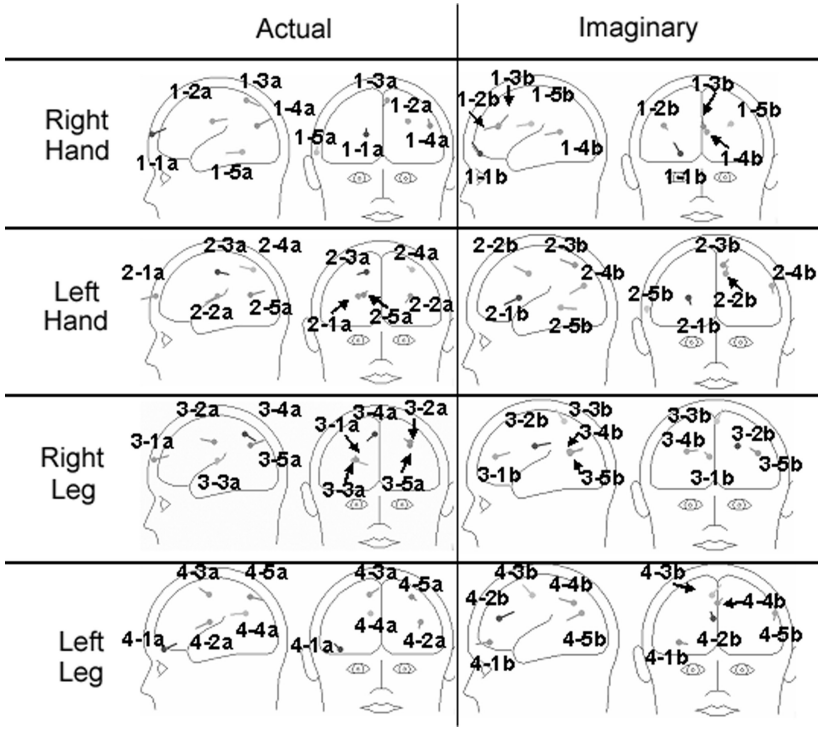

Figure 8. Location of sources during actual and imaginary movements with four limbs.

Brain-Source Activations

Cortical-source models for actual and imaginary movements with all four limbs are shown in Figure 8. Talairach coordinates of modeled cortical sources described in detail are shown in Table 2.

For actual movements of the right and left hands, we found activated brain sources in the contralateral motor cortex, SMA in the hand area (1–2a, 2–3a), the midline, and in the contralateral parietal cortex (1–3a, 2–4a), as well as in the ipsilateral frontal cortex (1–1a, 2–1a). For imaginary movements of the hands, we found similar sources in the contralateral motor cortex, SMA (1–5b, 2–2b), and in the parietal cortex (1–4b, 2–3b), which, however, were more anterior and lateral than for actual movement. We also observed more sources in the frontal cortex for imaginary-hand movements than for actual movements.

Table 2. Talairach coordinates of modeled cortical sources in Figure 8

Source number	x-loc	y-loc	z-loc	The nearest Brodman's area	The common name of the cortical area
1–1a	19.5	72.8	28.5	9 or 10	Prefrontal area
1–2a	−30.6	−12.3	35.7	6	Premotor or SMA
1–3a	−5.4	−62.3	57.9	5 or 7	Superior parietal lobule
1–1b	25.4	58.9	−0.13	10	Prefrontal area
1–3b	−1.8	30.8	31.7	6	Prefrontal area
1–4b	−6.3	−53.5	15.2	30	Parietal cortex
1–5b	−34.4	−14.9	29.9	6	Premotor or SMA
2–1a	27.7	69.7	29.1	10	Prefrontal area
2–3a	17.8	−20.5	51.1	6	Premotor or SMA
2–4a	−38.0	−71.0	48.4	3 or 1 or 2 or 5	Parietal cortex
2–1b	31.3	10.4	17.8	10	Prefrontal area
2–2b	−11.1	−4.7	46.3	24	Premotor or SMA
2–3b	−7.9	−66.3	49.5	7	Parietal cortex
3–2a	−38.2	−17.7	44.1	4	MI
3–2b	−25.9	−12.8	34.6	4	MI
4–3a	14.5	−14.1	57.9	4/6	MI/SMA
4–2b	5.0	37.2	30.8	9	Prefrontal area
4–3b	6.1	−9.0	55.0	6	Premotor/SMA

Moving the right and left legs was associated with cortical sources in the motor cortex (MI for the right leg (3–2a, 3–2b), SMA for the left leg (4–3a, 4–3b)), parietal cortex, and in the frontal cortex for both actual and imaginary movements. Imaginary leg movements exhibited more anterior cortical sources than those for actual movements (3–2b, 4–2b).

DISCUSSION

EEG Responses

In this study, we observed larger activations for actual movements than for imaginary movements which was in agreement with previous findings. Jankelowitz and Colebatch (2002) reported that actual movements were associated with larger amplitudes of movement-related cortical potentials.

Our whole-scalp time-frequency analysis showed that, for imaginary movements, there were large activations of the visual association cortex. A possible explanation is that visual imagination in humans actually involves the activation of sensory visual cortical areas, at least in tasks for which subjects were instructed to visualize moving their limbs (not kinesthetic mode of imagery) (Neuper, Scherer, Reiner, & Pfurtscheller, 2005).

Classification Method and Ways to Improve It

Several BCI studies published so far have exploited different aspects of imaginary movements with hands and legs (Gerking, Pfurtscheller, & Flyvbjerg, 2000; Guger, Edlinger, Harkam, Niedermayer, & Pfurtscheller, 2003; Neumann et al., 2001), and our results are in agreement with other studies on linear and nonlinear classification methods for BCI (Garrett, Peterson, Anderson, & Thaut, 2003). However, to our knowledge, there has been no successful attempt so far to classify EEG responses for four-limb imaginary movements. More than two dimensional BCI studies so far investigated imaginary tasks using the right hand, the left hand, the foot, and the tongue. Naeem, Brunner, Leeb, Graimann, and Pfurtscheller (2006) recorded EEG from 22 electrodes and applied independent component analysis, while Schlogl, Lee, Bischof, and Pfurtscheller (2005) recorded 60 channels of EEG and compared several classifiers.

Brain computer interface classification with a single-trial EEG has been investigated so far; however only one- or two-command classification has been achieved (Leuthardt, Schalk, Wolpaw, Ojemann, & Moran, 2004; Wolpaw & McFarland, 2004). Leuthardt et al. (2004) and Wolpaw and McFarland(2004) investigated single-trial classification for BCI in noninvasive or invasive recording. Single-trial based methods have shown high classification rates with short time for classification; however these methods also need long training sessions to establish the adaptive filtering for the classifier. For instance, Guger, Ramoser, and Pfurtscheller (2000) applied single-trial classification, but at least three-day training was required before the classification. We showed that in our four-command BCI system, we needed to prepare the template signals; however it took much less than three days. In addition, 10-trial averaging was able to improve the signal-to-noise ratio sufficiently to allow detection of the slight differences between the responses in four-limb movements (Kauhanen, Nykopp, & Sams, 2006).

In our analysis, the combined method using Time-Frequency RMS Error and Alpha–Beta-band (8–20 Hz) Time-Frequency RMS Error, selected among

all thirteen methods, achieved the best classification performance. However, it is important to note that when two analytical methods are used together, the way they are combined is essential, so that the result may not be a simple summation or multiplication, as demonstrated by the results shown in Table 1. Thus, in order to improve further the classification rates, it may be necessary to develop alternative approaches for combining analytical methods. As a next step, we will take advantage of classification methods such as goodness of fit, normalized parameters and two- or three-condition combinations. The classification method using RMS vector angles showed the worst result. This could be explained by the compression of information into a single value from 2.5 s data samples when using the RMS measure and into one angle value from five-dimensional vector norms.

The duration of each trial in our experiments was 5–8 s, therefore by using the current approach, a 60%–80% classification rate can be achieved within 50–80 s for four commands. It is possible to decrease the duration of each trial, which would contribute to decreasing the classification time. Qin, Ding, and He (2004) applied brain-source localization to classify right and left imaginary movements. We also may apply this method to improve the classification rate for right and left, however the usage of dipole computations for real-time classification is quite challenging. Also, we were unable to confirm the stability of source localization for hands and legs since the inverse solutions are not unique, especially at low signal-to-noise ratios. Moreover, although in this study we didn't focus on the preprocessing procedures necessary to eliminate the signal noise, prior denoising with independent component analysis (ICA) or laplacian filtering would help to increase the achieved classification rate (Vallabhaneni & He, 2004).

Recent reports demonstrated the important role of the type of the employed imaginary movements. Visual-motor and kinesthetic imagery showed different brain activations, with kinesthetic imagery achieving better classification rates than visual-motor imagery (Neuper, Scherer, Reiner, & Pfurtscheller, 2005). This means that also in four-limb BCI, it may be possible to obtain higher classification rates by applying precise task instructions of kinesthetic imagery to subjects.

Evaluating the evidence from the achieved classification rates, we concluded that the right hand is the most suitable limb to accomplish higher classification rates, compared to the left hand and to the right and left legs, although most previous BCI studies have made such an assumption by default.

Matching Analysis

Our results revealed further that leg movements showed smaller mismatch for A–A matching. A possible explanation for that finding is that these leg responses were more consistent over time (Figure 4) or that the hand potential variability (A–A mismatch) was larger due to fatigue or because the subject was still learning these movements.

For imaginary–imaginary (I–I) matching, the right limbs showed better consistency than the left ones. This could be because all subjects were right-handed, and it was easier for them to make imaginary movements with their dominant hands.

Finally, A–I matching for the right and left hands showed better template-test correspondence than for the legs. A possible reason may be that subjects were naturally able to achieve better imaginary movements with hand imagery than with leg imagery, in the sense that cortical activations were more similar to actual movements using the hands instead of the legs and it is easier to classify imaginary hand movements versus leg movements

The results of the transient matching analysis (I–I matching, Figure 6) indicate the possibility that the participants gradually became accustomed to the imaginary tasks after several dozens of trials, but after some time they suffered from fatigue and their concentration for imagination declined. An online neurofeedback procedure, which gives information to the subjects how the imaginary movement has been classified during the previous trial, could improve the classification results and reduce the subject fatigue.

Activated Brain Sources and Involved Cortical Areas

Comparisons between the four imaginary movements implied that the contralateral hemisphere controls the movement of body parts. Results from the source analysis showed that for imaginary limb movements more brain sources are located in the frontal cortex, as well as that sources in the motor cortex and in the parietal cortex are more anterior and lateral than for actual movements.

It is reported that activation in the frontal cortex was confined to the pre-motor and SMA cortices (Yahagi & Kasai, 1999). In addition, it is known that the parietal cortex has functions for somatosensory-motor association and sensory feedback from the muscles and joints during the execution of movements.

There has been a longstanding controversy in the scientific literature on the activation events during actual and imaginary movements, mainly about

the roles of the MI and the SMA. Although it has been thought that the SMA controls the preparation of movements and MI controls their execution (Clark, Tremblay, & Ste-Marie, 2004; Ersland et al., 1996), recent studies have found them to be interdependent (Lotze et al., 1999). In our results, we did not observe dipole activations in both SMA and MI, but activations were detected in only one of these cortical areas. This may also be the case because we analyzed EEG responses 96–500 ms after the visual cue, which includes mostly the preparation phase of the movements. Our results are in agreement with previous reports, showing activation in the SMA for imaginary movements.

In addition, we also observed activation in the MI even for imaginary right leg movements. Rodríguez et al. also showed MI activity during performance with motor imagery, showing broader and more intense cortical response modifications during motor tasks not accompanied by movements than during the execution of simple motor acts (Rodríguez et al., 2004). According to Lotze et al. (1999) several regional cerebral activations were measured using functional Magnetic Resonance Imaging (fMRI) during executed and imagined movements. The SMA, the premotor cortex, and the MI showed significant activations during both actual and imaginary movements. The somatosensory cortex (SI) was significantly activated only during actual movements. Thus, some studies using fMRI reported that the MI was also activated in imaginary movements. Amador and Fried (2004) investigated single-neuron activity in SMA, pre-SMA, and medial temporal lobe underlying preparation for action (Amador & Fried, 2004). Single-unit recordings were performed both during the execution and the mental imagery of finger apposition sequences. Only medial frontal neurons responded selectively to specific features of the motor plan. They observed similar patterns of activation during motor imagery and actual movement, but only neurons in the SMA differentiated between imagined and real movements.

In that way, the evidence from our results and the previously published data indicates that imaginary movements, depending on the target limb, involved activations in either the SMA or the MI.

CONCLUSIONS

In this study, we investigated EEG activities during actual and imaginary movements with four limbs in order to compare the properties of movement-related cortical potentials and to classify EEG responses during imaginary movements. Evoked potentials of imaginary movements exhibited slightly lower and delayed peak amplitudes in comparison to actual-movement responses, but

activations around the primary motor cortex and the supplementary motor cortex (SMA) were similar. Source analysis revealed the presence of brain sources in the motor cortex (mostly SMA) and in the parietal cortex even during imaginary movements. There were also more sources in the frontal cortex for imaginary than for actual movements.

The results of the four-command BCI classification using imagined limb-movement commands, indicated a 80% recognition rate for right-hand, 60% for left-hand, 60% for right-leg, and 70% for left-leg EEG responses, when a method using transient template matching to 10-trial test blocks and a time-frequency analysis was applied.

Using an imaginary-movement template matched to imaginary test data (I–I matching) showed a limb laterality dependency—right-limb responses were more consistent than left-limb ones. Furthermore, both A–I and A–A matching results showed dependencies on the limb type. While A–I matching demonstrated that imaginary movement responses were more similar to the actual-movement template for hands than for legs, A–A matching performance indicated that leg responses were more consistent than those for hands.

REFERENCES

Amador, N., & Fried, I. (2004). Single-neuron activity in the human supplementary motor area underlying preparation for action. *Journal of Neurosurgery*, *100*, 250–259.

Anderson, C. W., Stolz, E. A., & Shamsunder, S. (1998). Multivariate autoregressive models for classification of spontaneous electroencephalographic signals during mental tasks. *IEEE Transactions on Biomedical Engineering*, *45*, 277–286.

Brunner, C., Scherer, R., Graimann, B., Supp, G., & Pfurtscheller, G. (2006). Online control of a brain-computer interface using phase synchronization. *IEEE Transactions on Biomedical Engineering*, *53*, 2501–2506.

Clark, S., Tremblay, F., & Ste-Marie, D. (2004). Differential modulation of corticospinal excitability during observation, mental imagery and imitation of hand actions. *Neuropsychologia*, *42*, 105–112.

Ersland, L., Rosen, G., Lundervold, A., Smievoll, A. I., Tillung, T., Sundberg, H., et al. (1996). Phantom limb imaginary fingertapping causes primary motor cortex activation: an fMRI study. *Neuroreport*, *20*, 207–210.

Fadiga, L., Buccino, G., Craighero, L., Fogassi, L., Gallese, V., & Pavesi, G. (1999). Corticospinal excitability is specifically modulated by motor imagery: a magnetic stimulation study. *Neuropsychologia*, *37*, 147–158.

Filipovic, S. R., Sternic, N., Svetel, M., Dragasevic, N., Lecic, D., & Kostic, V. S. (2001). Bereitschaftspotential in depressed and non-depressed patients with Parkinson's disease. *Movement Disorders*, *16*, 294–300.

Garrett, D., Peterson, D. A., Anderson, C. W., & Thaut, M. H. (2003). Comparison of linear, nonlinear, and feature selection methods for EEG signal classification. *IEEE Transactions on Neural Systems and Rehabilitation Engineering*, *11*, 141–144.

Gerking, J. M., Pfurtscheller G., & Flyvbjerg, H. (2000). Classification of movement-related EEG in a memorized delay task experiment. *Clinical Neurophysiology*, *111*, 1353–1365.

Guger, C., Edlinger, G., Harkam, W., Niedermayer, I., & Pfurtscheller, G. (2003). How many people are able to operate an EEG-based brain-computer interface (BCI)? *IEEE Transactions on Neural Systems and Rehabilitation Engineering*, *11*, 145–147.

Guger, C., Ramoser, H., & Pfurtscheller, G. (2000). Real-time EEG analysis with subject-specific spatial patterns for a brain-computer interface (BCI). *IEEE Transactions on Rehabilitation Engineering*, *8*, 447–456.

Jankelowitz, S. K., & Colebatch, J. G. (2002). Movement-related potentials associated with self-paced, cued and imagined arm movements. *Experimental brain research*, *147*, 98–107.

Kauhanen, L., Nykopp, T., & Sams, M. (2006). Classification of single MEG trials related to left and right index finger movements. *Clinical Neurophysiology*, *117*, 430–439.

Leuthardt, E. C., Schalk, G., Wolpaw, J. R., Ojemann, J. G., & Moran, D.W. (2004). A brain-computer interface using electrocorticographic signals in humans. *Journal of Neural Engineering*, *1*, 63–71.2288;

Lotze, M., Montoya, P., Erb, M., Hulsmann, E., Flor, H., Klose, U., et al. (1999). Activation of cortical and cerebellar motor areas during executed and imagined hand movements: an fMRI study. *Journal of Cognitive Neuroscience*, *11*, 491–501.

Naeem, M., Brunner, C., Leeb, R., Graimann, B., & Pfurtscheller, G. (2006). Seperability of four-class motor imagery data using independent components analysis. *Journal of Neural Engineering*, *3*, 208–216.

Neumann, N., Kaiser, J., Kotchoubey, B., Hinterberger, T., & Birbaumer, N. P. (2001). Brain-computer communication: Self-regulation of slow cortical potentials for verbal communication. *Archives of Physical Medicine and Rehabilitation*, *82*, 1533–1539.

Neuper, C., Scherer, R., Reiner, M., & Pfurtscheller, G. (2005). Imagery of motor actions: Differential effects of kinesthetic and visual-motor mode of imagery in single-trial EEG. *Brain Research. Cognitive Brain Research*, *25*, 668–677.

Obermaier, B., Neuper, C., Guger, C., & Pfurtscheller, G. (2001). Information transfer rate in a five-classes brain-computer interface. *IEEE Transactions on Neural Systems and Rehabilitation Engineering*, *9*, 283–288.

Pham, M., Hinterberger, T., Neumann, N., Kubler, A., Hofmayer, N., Grether, A., et al. (2005). An auditory brain-computer interface based on the self-regulation of slow cortical potentials. *Neurorehabilitation and Neural Repair*, *19*, 206–218.

Pfurtscheller, G., Brunner, C., Schlogl, A., & Lopes da Silva, F.H. (2006). Mu rhythm (de)synchronization and EEG single-trial classification of different motor imagery tasks. *Neuroimage*, *31*, 153–159.

Pfurtscheller, G., & Lopes da Silva, F. H. (1999). Event-related EEG/MEG synchronization and desynchronization: basic principles. *Journal of Clinical Neurophysiology*, *110*, 1842–1857.

Platz, T., Kim, I. H., Pintschovius, H., Winter, T., Kieselbach, A., Villringer, K., et al. (2000). Multimodal EEG analysis in man suggests impairment-specific changes in movement-related electric brain activity after stroke. *Brain*, *123*, 2475–2490.

Qin, L., Ding, L., & He, B. (2004). Motor imagery classification by means of source analysis for brain-computer interface applications. *Journal of Neural Engineering*, *1*, 135–141.

Rodríguez, M., Muñiz, R., González, B., & Sabaté, M. (2004). Hand movement distribution in the motor cortex: The influence of a concurrent task and motor imagery. *Neuroimage*, *22*, 1480–1491.

Sellers, E. W., & Donchin E. (2006). A P300-based brain-computer interface: initial tests by ALS patients. *Clinical Neurophysiology*, *117*, 538–548.

Schlogl, A., Lee, F., Bischof, H., & Pfurtscheller, G. (2005). Characterization of four-class motor imagery EEG data for the BCI-competition 2005. *Journal of Neural Engineering*, *2*, 14–22.

Vallabhaneni, A., & He, B. (2004). Motor imagery task classification for brain computer interface applications using spatiotemporal principle component analysis. *Neurological research*, *26*, 282–287.

Wolpaw, J. R. & McFarland, D. J. (2004). Control of a two-dimensional movement signal by a noninvasive brain-computer interface in humans. *Proceedings of the National Academy of Sciences USA*, *101*, 17849–17854.

Wolpaw, J. R., Birbaumer, N., McFarland, D. J., Pfurtscheller, G., & Vaughan, T. M. (2002). Brain-computer interfaces for communication and control. *Journal of Clinical Neurophysiology*, *113*, 767–791.

Wolpaw, J. R., Birbaumer, N., Heetderks, W. J., McFarland, D. J., & Peckham, P. H. (2000). Brain-computer interface technology: a review of the first international meeting. *IEEE Transactions on Rehabilitation Engineering*, *8*, 164–173.

Yahagi, S., & Kasai, T. (1999). Motor evoked potentials induced by motor imagery reveal a functional asymmetry of cortical motor control in left- and right-handed human subjects. *Neuroscience Letters*, *276*, 185–188.

Yom-Tov, E., & Inbar, G. F. (2003). Detection of movement-related potentials from the electro-encephalogram for possible use in a brain-computer interface. *Medical and Biological Engineering and Computing*, *41*, 85–93.